ISSN 1067-8212, Russian Journal of Non-Ferrous Metals, 2022, Vol. 63, No. 6, pp. 690–700. © Allerton Press, Inc., 2022.

PHYSICAL METALLURGY AND HEAT TREATMENT

Thermal Modeling of Tool-Work Interface during Friction Stir Welding Process

A. Chikh[a], *, M. Serier[b], **, R. Al-Sabur[c], *, A. N. Siddiquee[d], ****, and N. Gangil[e], *******

[a] *Department of Mechanical Engineering, Institute of Technology, University of Relizane, Algiers, Algeria*

[b] *Department of Civil Engineering, Institute of Technology, University of Relizane, Algiers, Algeria*

[c] *Mechanical Department, Engineering College, University of Basrah, Basrah, Iraq*

[d] *Department of Mechanical Engineering, Jamia Millia Islamia, New Delhi, 110025 India*

[e] *Department of Mechanical Engineering, Ajay Kumar Garg Engineering College, Ghaziabad, Uttar Pradesh, 201009 India*

**e-mail: aminachikh10@yahoo.com*

***e-mail: mohamed.serier@cu-relizane.dz*

****e-mail: raheem.musawel@uobasrah.edu.iq*

*****e-mail: arshadnsiddiqui@gmail.com*

******e-mail: namrata.gangil@gmail.com*

Received January 19, 2022; revised July 18, 2022; accepted July 26, 2022

Abstract—Adequate heat input provided by the proper combination of friction stir welding (FSW) parameters is critical to sound welding. Optimum parameter setting requires exhaustive trials and extensive experiments, which require considerable time, resources, and cost. This study uses simulation and modelling approaches to generate three significant tool-work heat flux generating interfaces (tool shoulder, lateral and bottom surfaces of the pin). The temperature data was acquired by performing nine experiments on 4 mm thick AA6060-T5 sheets. The effects of significant FSW parameters (Tool Rotational Speed (TRS) and welding speed (WS)) on the heat input were modelled. The calculated heat input rates at the shoulder and pin surfaces (Q_1, Q_2, and Q_3) were numerically estimated. The experimental data was converted into a mathematical model using the response surface method to study the effect of welding parameters on heat input from each of the three surfaces. The analysis of the results showed that among three interfaces, the shoulder provides the most significant heat input due to the immense friction between this surface and the parts to be welded. The interaction between the main factors produced little heat on the three surfaces. The ANOVA test showed that the three models are a good approximation of the results of both experiments and theories.

Keywords: friction stir welding, aluminum alloys, welding parameters, contact parts/tool

DOI: 10.3103/S1067821222060049

INTRODUCTION

Friction stir welding (FSW) is a recent and promising joining method. Although the inception of FSW was initially intended for age-hardened aluminum alloys, it has now evolved as a promising process to weld almost all metals/alloys and polymers [1]. FSW utilizes friction heat to soften the base materials and consolidate the joint by stirring and mixing the softened material. A rotating cylindrical tool with a pin at its ends penetrates the base materials until the pin is fully inserted into the plates. The shoulder of the rotating tool contacts the surface [2, 3].

The pin stirs and mixes the plasticized material and consolidates the joint. On the other hand, the shoulder is the major source of frictional heat input. Effective joining and a sound weld rely considerably on knowledge of the phenomena involved and the effect of the various process parameters. Simulation and modeling are essential tools for accurately predicting welding conditions and saving significant effort, time, and resources. Consequently, several numerical simulations on various aspects, considering the thermal or thermomechanical aspect, have been reported [4].

Theoretical and experimental studies have demonstrated the phenomena of heat input and heat transfer, thermal field, and the material flow during FSW of aluminum alloys [5–7]. Some of the studies extended to be real time monitoring of the heat and temperature along the welding line and heat effected zone [8]. Zhang et al. [9] presented a transient thermal model that takes into account all of the FSW periods for give better understand the FSW process. In this study the heat generation rate is estimated using a temperature-dependent apparent friction coefficient computed using the inverse solution technique. Tang et al showed that the temperature distribution is symmetri-

cal about the weld line, and the peak temperature existing at the center of the plate was estimated to be around 450°C [10]. Song and Kovacevic [11, 12] have experimentally determined that the coefficient of friction has a direct and more significant impact on the quantity of heat generated and, therefore, on the peak temperature reached in the joint. However, an analysis of heat transfer during the process, performed by Nandan et al. [13] quantified the amount of energy supplied to the plate. Temperature measurements by thermocouples were taken inside the tool and in the thickness of the plate. An inverse numerical method is used to optimize the heat fluxes to the plate based on the measurements of these experiments [14]. Modern modeling tools' ever-increasing capabilities have aided in significant insights into heat input, heat and material flow, and their effects on joint quality. The industry has reaped significant benefits from modeling thermal flow fields, and the process has evolved as a versatile technology for complete welding solutions for most materials. Unfortunately, the assumptions made during modeling may significantly deviate from the actual process conditions, and consequently, predictions from the model often widely deviate from the actual practice. The work focusing on modeling coupled with experimental validation is essential to developing robust built-in modules that are critical to enhancing the model's output reliability. The computed temperatures, for example, do not always agree with the measured ones [15]. One of the reasons may be that the heat lost through the tool was not adequately accounted for. In a typical investigation, the amount of heat transmitted to the tool was about 5% of the total energy expended. Serier et al. [16] proposed a tool with a vibrating shoulder that reduces heat leakage from the shoulder during the welding process. In the present article, modeling, and numerical simulation for the heat transfer from the tool and the sheets being welded have been performed. The heat input from the three surfaces, i.e., (i) shoulder, (ii) lateral surface of the pin, and (iii) bottom surface of the pin, was considered. The present study results are expected to lead to better utilization of the supplied energy, enhance the energy efficiency of the process, and improve the weld quality. A response surface methodology (RSM) optimization of the heat flow is also attempted to ensure good welding quality.

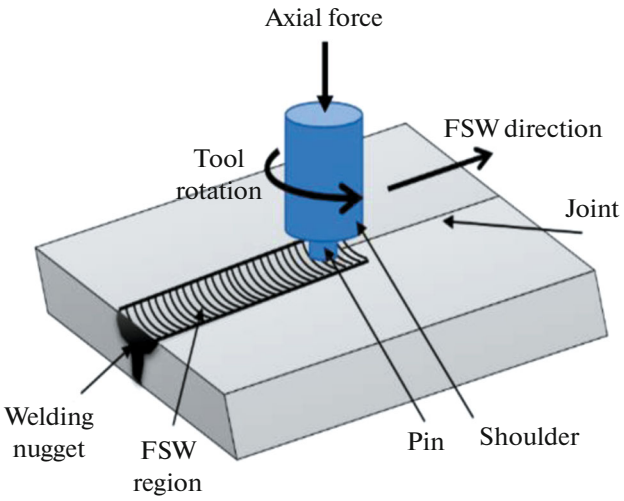

Fig. 1. Schematic of FSW process [17].

MATERIALS, METHOD, AND ANALYSIS

The AA6060-T5 sheets of 200 × 50 × 4.25 mm^3 size were used as a base material (refer to Fig. 1). The elemental composition of the alloy and its properties are presented in Tables 1 and 2, respectively.

The HCHCr (typical composition given in Table 3), the FSW tool employed in this work (refer to Fig. 2), is comprised of a 14 mm shoulder diameter with a threaded cylindrical pin having 6 mm diameter and 4 mm height.

Table 1. Chemical composition of AA6060-T5 aluminum alloy (%)

%	Si	Fe	Cu	Mn	Mg	Cr	Zn	Ti
Min	0.03	0.10			0.35			
Max	0.60	0.30	0.10	0.10	0.60	0.05	0.15	0.10

Table 2. Mechanical properties of AA6060-T5 aluminum alloy

E, MPa	R_p, MPa	A, %	ν	d, g/cm^3	Fusion, °C	λ, W/m °C	C_p, J/kg °C
69500	110	150	14	0.33	2.70	605–665	200

Table 3. Chemical composition (wt %) of HCHCr tool material

C	Si	Mn	P max	S max	Cr
1.9–2.2	0.1–0.6	0.2–0.6	0.03	0.03	11–13

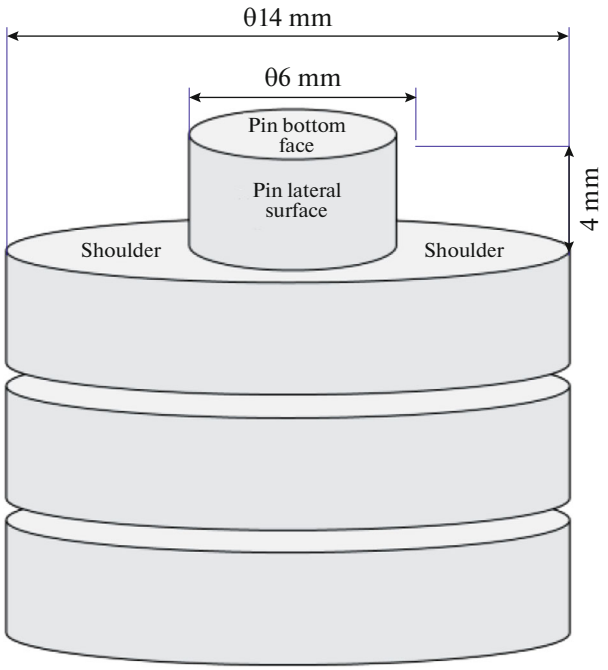

Fig. 2. Regions/interfaces of Energies input and the tool geometry of FSW process.

On a vertical milling machine, the FSW experiments were carried out. Nine experiments with two factors, both at level three, were selected to perform the experiments (refer to Table 4). Two parameters that significantly affect FSW, i.e., Tool Rotational Speed (TRS) and welding velocity (WS) were chosen according to the available literature and our previous work. The TRS varied between 200 and 600 RPM, and the WS was in the range of 0.5 to 1.5 mm/s. For a sufficient understanding of the heat input and heat transfer during the process, the temperatures were measured via thermocouples on the two base metal sheets (Fig. 3)

Thermocouples used in this study were placed at 15 mm from the center of the faying surface (Fig. 3).

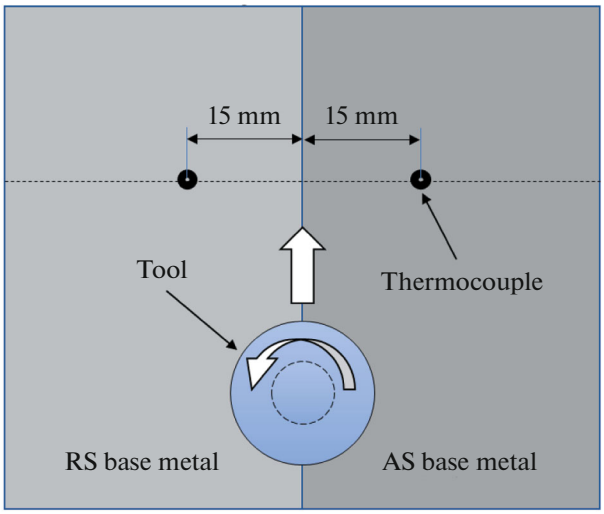

Fig. 3. Thermocouple positions on both sides of the faying surface.

The temperature values for each experiment are also given in Table 4.

The analytical heat input model consists of the identification of substantial heat tool-material input interfaces during FSW. Three interfaces Q_1, Q_2, and Q_3, are identified. The adequacy of heat input is essential for the sound joint and evolution of the mechanical properties of FSW welds. The modeling is based on the following essential data:

(1) The contact shear stress "$\tau_{contact}$" is uniform.

(2) The shear-assisted stirring occurs at the intimate interface only.

(3) The plastic deformation during stirring was considered to contribute heat through atomic friction.

(4) During the current friction process, the value of the interfacial shear resulting from the contact and the friction is equal, so the $\tau_{contact} = \tau_{friction} = \mu\rho = \mu\sigma$ while the stress $\sigma = F_f/A$ here, A: tool contact area, σ: contact pressure, μ *is* friction coefficient, ρ: density,

Table 4. Temperature obtained by experimental tests

Exp.	WS, mm/s	TRS, rpm	Temperature, K
01	0.5	200	700.2
02	0.75	200	694.4
03	1.5	200	688.2
04	0.5	300	762.7
05	0.75	300	756.0
06	1.5	300	749.6
07	0.5	600	807.4
08	0.75	600	801.5
09	1.5	600	797.3

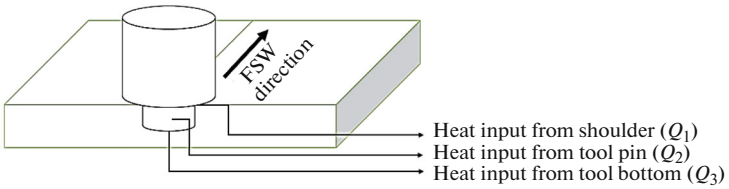

Fig. 4. Heat generation zones between parts and tool.

F_f: forging force which was regarded from the outset in the initial heat quantities.

(5) The deviation of the interface area between the shoulder and the pin is viewed in equations Q_1, Q_2, and Q_3.

(6) The model does not consider convective heat transfer, which may be a part of the process.

Based on the thickness of the material, the shape of the tool, and the depth of the plunge used in this study, an 8 kN forging force was considered [18].

As shown in Fig. 4, the total heat input (QT) constitutes the sum of heat inputs from the three. It was estimated according to Eqs. (2), (4), and (6) [19].

Heat input from the shoulder interface (i.e., Q_1) is given by (Eq. (1)):

$$Q_1 = \int_0^{2\pi}\int_{R_{hp}}^{R_s} wr^2\mu\sigma d\theta dr, \quad (1)$$

$$Q_1 = \frac{2}{3}w\mu\frac{F_f}{(R_s - R_{hp})^2}\left(R_s^3 - R_{hp}^3\right). \quad (2)$$

Heat input from the lateral interface (i.e., Q_2) of the pin is given by (Eq. (3)):

$$Q_2 = \int_0^{2\pi}\int_0^{1} wr^2\mu\sigma d\theta dz, \quad (3)$$

$$Q_2 = 2\pi w\mu H_p\left(\frac{R_{hp}}{2}\right)^2. \quad (4)$$

Heat input from the pin bottom interface (i.e., Q_3) is given by (Eq. (5)):

$$Q_3 = \int_0^{2\pi}\int_0^{R_{hp}} wr^2\mu\sigma dr d\theta, \quad (5)$$

$$Q_3 = \frac{2}{3}w\mu F_f R_{hp}. \quad (6)$$

Thus, the Q_T, can be deduced as the sum of heat inputs from the three interfaces as follows

$$Q_T = Q_1 + Q_2 + Q_3, \quad (7)$$

Table 5. Nomenclatures for thermos-mechanical modeling

Nomenclature	Units	Description
cp	J/kg K	Specific heat capacity
dA	–	Infinitesimal area
dF_f	–	Infinitesimal forging force
$d\theta$	–	Infinitesimal angular
dr	–	Infinitesimal radius
dQ	–	Infinitesimal heat generation
H_p	mm	Tool probe height
K	W/m K	Thermal conductivity
R_{hp}	mm	Tool probe radius
R_s	mm	Tool shoulder radius
t	mm	Thickness workpiece
TRS	rpm	Tool rotational speed
WS	mm/s	Welding speed
ω	rad/s	Tool angular rotation speed
ϑ	m/s	Transverse tool speed of ωr
α	W/m K	Thermal diffusivity

Table 6. Temperature and heat input obtained by simulation

Exp.	WS, mm/s	TRS, rpm	Heat input from			Temperature, K
			shoulder Q_1, kW	tool pin Q_2, W	tool bottom Q_3, W	
01	0.5	200	2.97	250.1	45.6	700.2
02	0.75	200	3.05	252.8	46.1	694.4
03	1.5	200	3.17	258.5	47.7	688.2
04	0.5	300	3.72	213.9	61.9	762.7
05	0.75	300	3.72	215.5	62.1	756.0
06	1.5	300	3.88	216.2	63.4	749.6
07	0.5	600	4.23	164.3	76.2	807.4
08	0.75	600	4.31	168.1	77.0	801.5
09	1.5	600	4.47	172.3	77.4	797.3

$$Q_T = w\mu F_f \left\{ \frac{2}{3} \left[\frac{\left(R_s^3 - R_{hp}^3\right)}{\left(R_s - R_{hp}\right)^2} + R_{hp} \right] + \frac{H_p}{2} \right\}. \quad (8)$$

The heat input as given by Eq. (8) can be further developed to obtain a total heat input per unit length. Equation (9) [19] can be used to find the total heat input for a unit of weld length when the sliding contact condition is taken into account:

$$Q_T = \frac{w\mu F_f}{\vartheta} \left\{ \frac{2}{3} \left[\frac{\left(R_s^3 - R_{hp}^3\right)}{\left(R_s - R_{hp}\right)^2} + R_{hp} \right] + \frac{H_p}{2} \right\}. \quad (9)$$

Effective energy for a unit length of the weld is estimated as per Eq. (1) as a ratio of the length of pin length Hp to plate thickness "t" and multiplying it by energy per unit length of the weld (as given in Eq. (10)) [19].

$$Q_{eff} = \left(\frac{H_p}{t} \right) Q_{\frac{E}{wl}}. \quad (10)$$

The welding temperature (T_w), solidus temperature (T_s), and effective energy per unit weld length are empirically related as per (Eq. (11)) [19].

$$\frac{T_w}{T_s} = \alpha Q_{eff} + \left(\frac{\mu R_{hp}}{R_{hp}} \right), \quad (11)$$

where,

$$\alpha = \frac{K}{c_p \rho}.$$

The calculation was performed by considering three faces of the tool that contributed to heat input, as shown in Fig. 4. Table 6 gives the calculation result, representing the temperature and heat input from each interface. The notations are Q_1 represents the heat input from the shoulder surface; Q_2 represents the heat input from the pin's lateral surface; and Q_3 represents the heat input from the bottom of the pin (as given in Table 4).

The orthogonal array (OA), as given in Table 7, represents the coded levels of the parameters [20, 21]. According to the standard procedures for every parameter, the highest level is coded as "+1", the lowest level is coded as "–1", and the intermediate level is coded "±1". The values of factors are expressed within different ranges. They are normalized to convert them within a common range to be comparable (normalization can be done as per (Eq. (12)):

$$X_i = \left[u_i - (u_{min} + u_{max})/2 \right] / (u_{max} - u_{min})/2. \quad (12)$$

The levels of parameters as given in Table 6 were coded using Eq. (12), and the obtained coded values are given in Table 7.

The numerical analysis for the estimation was performed using least squares. A second-degree polynomial was considered, and higher-order terms were neglected. The squared terms are usually sufficient to depict surface curves. Equation (13) is the general form of the polynomial model.

$$y_i = a_0 + \sum_{i=1}^{k} x_i a_i + \sum_{i=1}^{k} a_{ii} x_i^2 + \sum_{i=1}^{k-1} \sum_{i=j=1}^{k} I_{ij} x_i x_j. \quad (13)$$

The developed form of Eq. (12) for three parameters is given by (Eq. (13)):

$$y_i = a_0 + x_{i1} a_1 + x_{i2} a_2 + I_{12} x_{i1} x_{i2} + x_{i1}^2 a_{11} + x_{i2}^2 a_{22} + e_i. \quad (14)$$

Knowing that term e_i represents the difference between the experimental value and that given by the polynomial, and that I_{12} is the interaction between

Table 7. Temperature and heat input obtained by simulation

Exp.	WS, mm/s	TRS (RPM)	Predicted heat input from		
			shoulder Q_1, kW	tool pin Q_2, W	tool bottom Q_3, W
01	−1	−1	2.97	250.1	45.6
02	−0.5	−1	3.05	252.8	46.1
03	1	−1	3.17	258.5	47.7
04	−1	−0.5	3.72	213.9	61.9
05	−0.5	−0.5	3.72	215.5	62.1
06	1	−0.5	3.88	216.2	63.4
07	−1	1	4.23	164.3	76.2
08	−0.5	1	4.31	168.1	77.0
09	1	1	4.47	172.3	77.4

variables. A matrix can be developed as given below when applying this to the nine experimental sets:

$$\begin{pmatrix} y_1 \\ y_2 \\ y_3 \\ y_4 \\ y_5 \\ y_6 \\ y_7 \\ y_8 \\ y_9 \end{pmatrix} = \begin{pmatrix} 1 & x_{1.1} & x_{1.2} & x_{1.1}\times x_{1.2} & x_{1.1}^2 & x_{1.2}^2 \\ 1 & x_{2.1} & x_{2.2} & x_{2.1}\times x_{2.2} & x_{2.1}^2 & x_{2.2}^2 \\ 1 & x_{3.1} & x_{3.2} & x_{3.1}\times x_{3.2} & x_{3.1}^2 & x_{3.2}^2 \\ 1 & x_{4.1} & x_{4.2} & x_{4.1}\times x_{4.2} & x_{4.1}^2 & x_{4.2}^2 \\ 1 & x_{5.1} & x_{5.2} & x_{5.1}\times x_{5.2} & x_{5.1}^2 & x_{5.2}^2 \\ 1 & x_{6.1} & x_{6.2} & x_{6.1}\times x_{6.2} & x_{6.1}^2 & x_{6.2}^2 \\ 1 & x_{7.1} & x_{7.2} & x_{7.1}\times x_{7.2} & x_{7.1}^2 & x_{7.2}^2 \\ 1 & x_{8.1} & x_{8.2} & x_{8.1}\times x_{8.2} & x_{8.1}^2 & x_{8.2}^2 \\ 1 & x_{9.1} & x_{9.2} & x_{9.1}\times x_{9.2} & x_{9.1}^2 & x_{9.2}^2 \end{pmatrix} \begin{pmatrix} a_0 \\ a_1 \\ a_2 \\ I_{1.2} \\ a_{1.1} \\ a_{2.2} \end{pmatrix} + \begin{pmatrix} e_1 \\ e_2 \\ e_3 \\ e_4 \\ e_5 \\ e_6 \\ e_7 \\ e_8 \\ e_9 \end{pmatrix}.$$

The coefficients are found by Eq. (15).

$$\text{Coefficients} = (X^t X)^{-1}(X^t)(Y). \quad (15)$$

Because the current work has concentrated on three outputs (Q_1, Q_2, and Q_3), three polynomials must be formulated so that each polynomial has its own factors by applying Eq. (15) to heat input from the shoulder, lateral surface of the pin, and bottom face of the pin.

Table 8. The values of the polynomial coefficients for each of the three areas of the tool

Factor	Heat input from		
	shoulder Q_1, kW	shoulder Q_1, kW	shoulder Q_1, kW
a_0	4.24	189.74	73.09
a_1	0.102	3.16	0.75
a_2	0.638	−2.73	15.15
I_{12}	0.013	0.27	−0.24
a_{11}	−0.004	−1.52	15.15
a_{22}	−0.522	22.94	−0.13
a_0	4.24	189.74	73.09

The three polynomials can be written as follows (Eq. (16) through (18)):

(i) Heat Input from Shoulder (Q_1)

$$y_i = 4.24 + 0.102X_1 + 0.638X_2 + 0.013X_1X_2 - 0.004X_1^2 - 0.522X_2^2 + e_i. \quad (16)$$

(ii) Heat Input from lateral surface of Pin (Q_2)

$$y_i = 189.74 + 3.16X_1 - 42.73X_2 + 0.27X_1X_2 - 1.524X_1^2 + 22.94X_2^2 + e_i. \quad (17)$$

(iii) Heat Input from the bottom face of the pin (Q_3)

$$y_i = 73.09 + 0.75X_1 + 15.15X_2 - 0.24X_1X_2 + 15.15X_1^2 - 0.13X_2^2 + e_i. \quad (18)$$

The RSM was used to predict the maximum at the three effective welding surfaces and determine the extent of the effect of the two FSW parameters and their interaction effect (Table 8) on the temperature.

RESIDUAL ANALYSIS

The adequacy and accuracy of the model can be diagnosed by residuals versus predicted values and typical probability plots. The plots represent the deviations between the predicted and experimental values. The presence of a regular pattern of residuals shows that the model is insufficient. For an adequate and accurate model, the residuals in a typical probability plot are arranged about a straight line (Fig. 5).

The straight-line confirms that the model is sufficient and accurate. Furthermore, the ANOVA test further confirms that the developed model is adequate. The value of the F_{crit} test, taken at $(k - 1)$ from the Fischer table, and the value calculated from the model

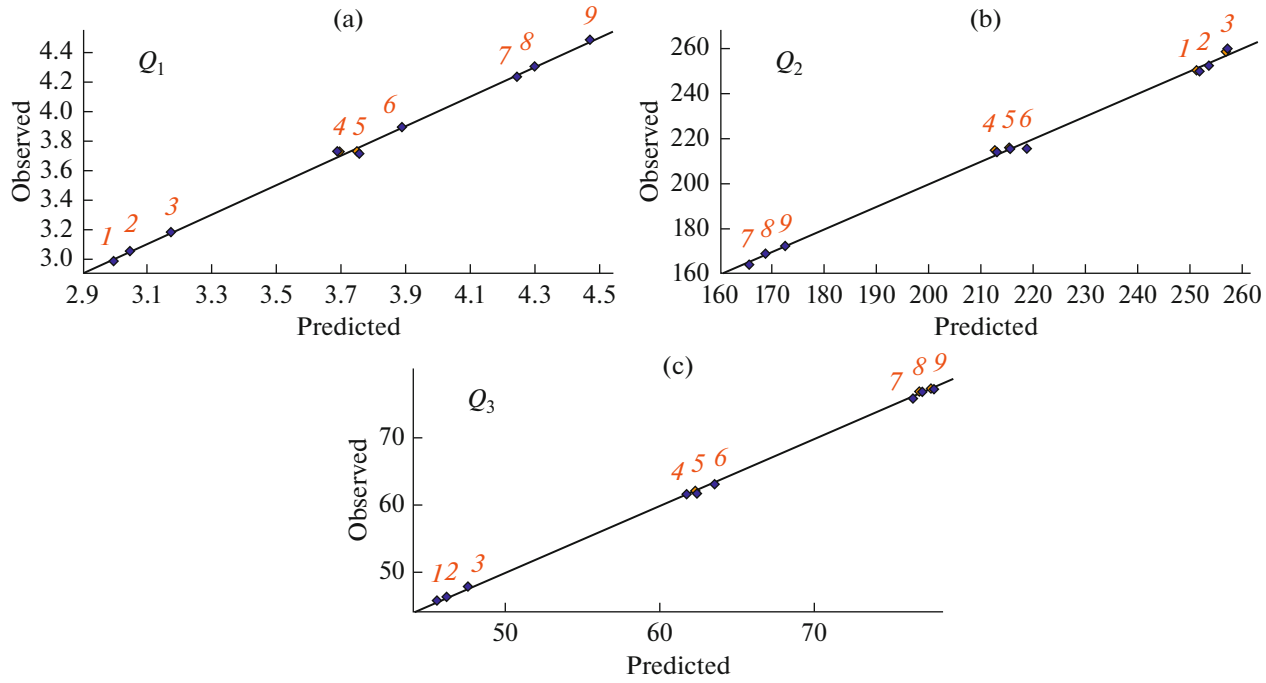

Fig. 5. Heat Schematic of both models (experimental and theoretical), (a) Both models heat Input from Shoulder (Q_1), (b) Both models Heat Input from tool Pin (Q_2), and (c) Both model heat Input from tool Bottom (Q_3).

(F_{abs}). The model is globally significant, and if $F_{abs} > F_{crit}$, As a result, this model has global significance if $F_{abs} \ggg F_{crit}$. It means the model is excellent. For the degrees of freedom, we extract a F_{crit} value equal to 9.01, so the three models (Tables 9–11) are excellent, as shown in Fig. 4, and the experimental models are identical to the theoretical models.

Influence of the WS on the Heat Input from the Three Surfaces

The main effects plots are given in Fig. 6a. It can be noted from the plots that the WS maintains almost similar effects on the three surfaces of the tool. It indicates that an increase in speed increases the heat input rate, reducing the temperature. Furthermore, the slopes of individual plots in Fig. 6a also suggest that the WS has a more significant effect on the heat input from the shoulder than on the other two surfaces. On the other hand, the effect of the TRS, as shown in Fig. 6b, shows that the plot is similar for the heat input from the shoulder and bottom of the pin. Whereas its effect is opposite to the heat input from the lateral surface of the pin, this peculiar characteristic indicates that an increase in TRS enhances the heat input from the shoulder and bottom and the bottom surface of the pin. However, the heat input from the lateral surface of the pin reduces as the TRS is increased. This peculiarity may be attributed to the fact that the material movement while stirring action of the pin follows a stick-and-slip action; with the increase in TRS, the frequency of stick and slip increases, and net heat input is reduced.

Simultaneous Effect of Weld Speed and Tool Rotational Speed

The effect of heat input due to secondary factors (interaction effect) is based on the response's simultaneous variation of two factors. Their effects may be

Table 9. ANOVA for heat input from shoulder (Q_1)

Variation source	ddl	Sum of squares	Mean squares	F_{abs}
Regression (model)	$(k-1):5$	SCEL = 2.51003	MCF = SCEL/$(k-1)$ 0.50	MCF/MCR 734
Residuals	$(n-k):3$	SCER = 0.002	MCR = SCER/$(n-k)$ 0.0006	
Total	$(n-1):8$			

Table 10. ANOVA for heat input from tool pin (Q_2)

Variation source	ddl	Sum of squares	Mean squares	F_{abs}
Regression (model)	$(k-1):5$	SCEL = 1391.82	MCF = SCEL/$(k-1)$ 278.364	MCF/MCR 4579.65
Residuals	$(n-k):3$	SCER = 0.182348	MCR = SCER/$(n-k)$ 0.0607827	
Total	$(n-1):8$			

Table 11. ANOVA for heat input from tool bottom (Q_3)

Variation source	ddl	Sum of squares	Mean squares	F_{abs}
Regression (model)	$(k-1):5$	SCEL = 11076.5	MCF = SCEL/$(k-1)$ 2215.29	MCF/MCR 527.037
Residuals	$(n-k):3$	SCER = 12.6099	MCR = SCER/$(n-k)$ 4.20329	
Total	$(n-1):8$			

similar or opposite in magnitude and nature. The results are defined in two ways: one in space using a curved spatial surface, and the other in the form of contour maps using a surface projection termed responses curve. These two combined representations are derived from Eqs. (16)–(18) and are represented in Figs. 7 and 8.

The continuous variation of data presented in the surface plot (Fig. 7) and contour maps (as given in Fig. 8) can be more effectively represented, interpreted, and analyzed when the data from these plots and maps is visualized through the tabulated data.

Table 12 shows the temperature values at the shoulder under the influence of the various parameters. It can be noted that the interaction gives the greatest value of heat input (i.e., approximately 4.68) when both the speeds are at their highest levels, and this heat shrinks (to a value of 3.07) when both speeds are at their lowest levels.

Furthermore, Table 13 gives the heat input rate at the lateral surface of the pin. The data values denote

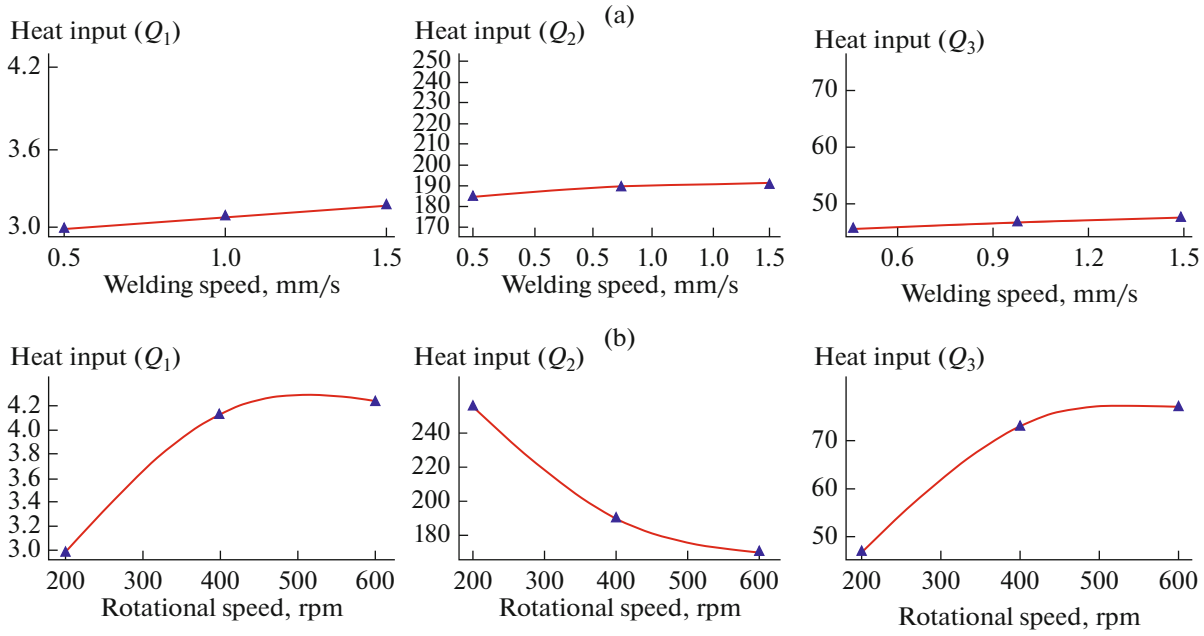

Fig. 6. Representation of the effects of the main factors with: (a) effect of WS and (b) effect of TRS.

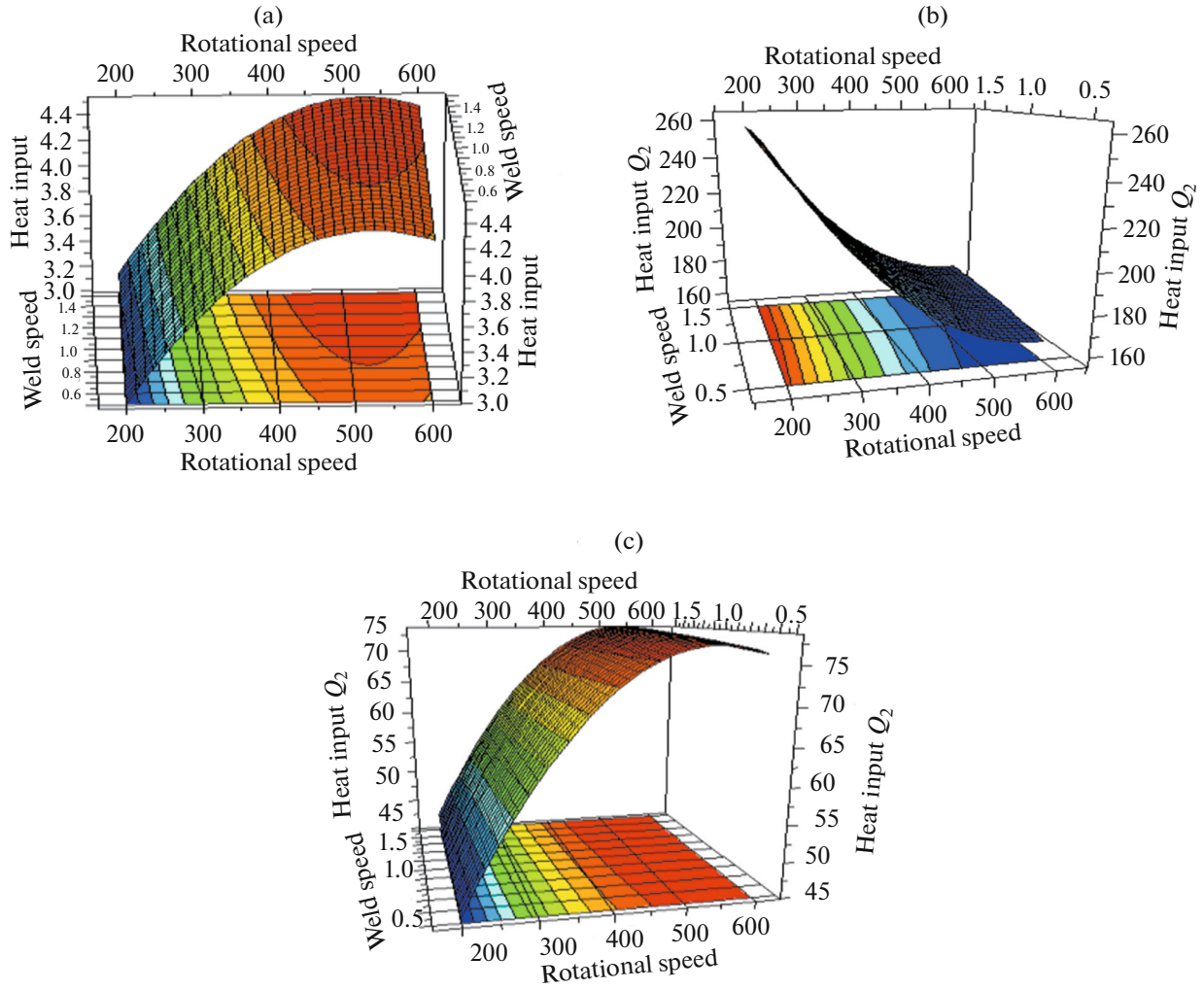

Fig. 7. Response variation according to WS and TRS.

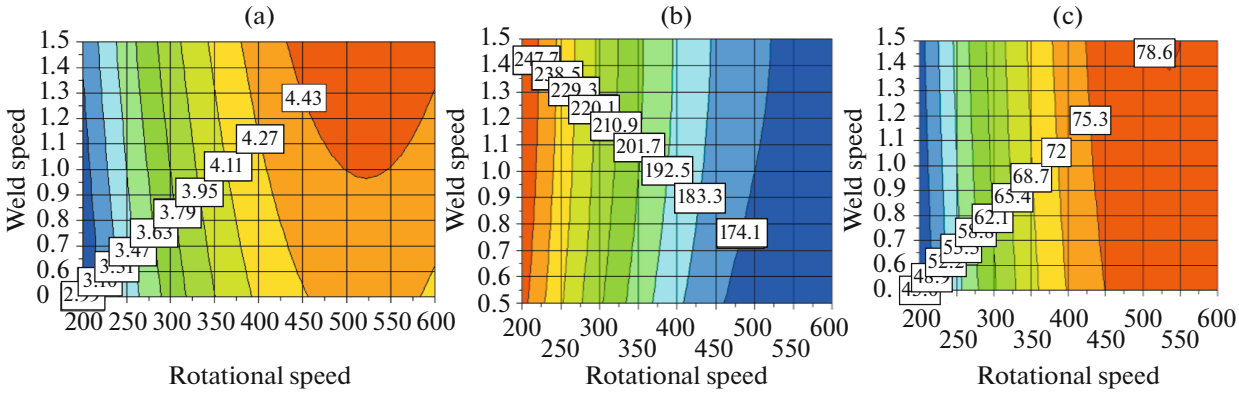

Fig. 8. Responses curves according of response variation.

that the heat input attains its greatest value (i.e., 254 W) when the WS is at its highest level, and the TRS is at its lowest level. The heat generation value attains the lowest value (i.e., 165 W) when the TRS is at its highest and the WS is at its lowest level.

Finally, Table 14 depicts the heat input percentage from the bottom of the pin, or what may be termed as the maximum immersion of the tool in the material. This point is significant for FSW because it is the reason for the conduction of the consolidation at the

Table 12. Results of different parameter values for heat input from shoulder (Q_1)

TRS, rpm	WS (0.5 mm/s)	WS (0.75 mm/s)	WS (1.5 mm/s)
200 RPM	3.07	3.11	3.25
300 RPM	3.69	3.74	3.69
600 RPM	4.25	4.31	4.68

Table 13. Results of different parameter values for heat input from tool pin (Q_2)

TRS, rpm	WS (0.5 mm/s)	WS (0.75 mm/s)	WS (1.5 mm/s)
200 RPM	250	249	254
300 RPM	211	210	220
600 RPM	165	167	172

Table 14. Results of different parameter values for heat input from tool bottom (Q_3)

TRS, rpm	WS (0.5 mm/s)	WS (0.75 mm/s)	WS (1.5 mm/s)
200 RPM	45.6	47	48
300 RPM	62	63	63.2
600 RPM	74	75	77.7

coldest part of the base materials (i.e., "at the back side of the two sheets to be welded"). Thus, the combination of speeds that gives more heat input in this sensitive area can be considered desirable. Going by this, it can be noted that the most favorable combination of speeds is the one that gives more heat generation in this sensitive area, and it is at 600 rpm TRS with a 1.5 mm/s WS. Furthermore, an examination of the contour maps (i.e., Fig. 8c) reveals that the highest value achievable in this area is nearly 79 at a TRS of 525 rpm and a WS of 1.5 mm/s.

CONCLUSIONS

The main factor for sound friction stir welded joints is adequate heat input. In turn, the amount of heat input depends on many characteristics, including material thickness, the metallurgy of based materials being among the critical factors. Modeling and simulation are essential tools that can be used to gauge the desired results and save material, time, and costs associated with trial experiments. This experimental work has predicted heat input from the significant tool-base metal interface. Based on the investigation, the following conclusions were drawn:

(1) The heat input models for the three interfaces, i.e., tool shoulder, lateral surface of the pin, and bottom face of the pin, were subjected to an ANOVA test. This test has proven that the models are accurate and reliable and can help predict further results in the field of study.

(2) The study results show that the effect of WS is small on the heat input from the three interfaces, and the TRS remains the primary factor affecting the major amount of heat input.

(3) The study results show that the tool shoulder contributes between 80 and 90% of the heat input, depending on the welding conditions. The remaining amount of heat input is contributed by tool surfaces.

CONFLICT OF INTEREST

The authors declare that they have no conflicts of interest.

REFERENCES

1. Emamian, S., Awang, M., Yusof, F., Hussain, P., Meyghani, B., and Zafar, A., The effect of pin profiles and process parameters on temperature and tensile strength in friction stir welding of AL6061 alloy, in *The Advances in Joining Technology,* Springer, 2019, pp. 15–37. https://doi.org/10.1007/978-981-10-9041-7_2
2. Gangil, N., Maheshwari, S., and Siddiquee, A.N., Influence of tool pin and shoulder geometries on microstructure of friction stir processed AA6063/SiC composites, *Mech. Ind.,* 2018, vol. 19, no. 2, p. 211. https://doi.org/10.1051/meca/2018010
3. Asmare, A., Al-Sabur, R., and Messele, E., Experimental investigation of friction stir welding on 6061-T6 aluminum alloy using Taguchi-Based GRA, *Metals,* 2020, vol. 10, no. 11, p. 1480. https://doi.org/10.3390/met10111480
4. Liu, X., Yu, Y., Yang, S., and Liu, H., A modified analytical heat source model for numerical simulation of temperature field in friction stir welding, *Adv. Mater. Sci. Eng.,* 2020, vol. 2020, p. 4639382. https://doi.org/10.1155/2020/4639382
5. Shaik, B., Gowd, G.H., and Durgaprasad, B., Experimental investigations on friction stir welding process to join aluminum alloys, *Int. J. Appl. Eng. Res.,* 2018, vol. 13, no. 15, pp. 12331–12339.
6. Khalaf, H.I., Al-Sabur, R., Abdullah, M.E., Kubit, A., and Derazkola, H.A., Effects of underwater friction stir welding heat generation on residual stress of AA6068-T6 aluminum alloy, *Materials,* 2022, vol. 15, no. 6, p. 2223. https://doi.org/10.3390/ma15062223
7. Siddiquee, A.N., Pandey, S., Abidi, M.H., AlAhmari, A., Khan, N.Z., and Gangil, N., Microstructural characterization and in-process traverse force during friction stir welding of austenitic stainless steel, *Proc. Inst. Mech. Eng., Part C,* 2020, vol. 234, no. 5, pp. 1031–1043. https://doi.org/10.1177/0954406219888238
8. Al-Sabur, R., Jassim, A.K., and Messele, E., Real-time monitoring applied to optimize friction stir spot welding joint for AA1230 Al-alloys, *Mater. Today: Proc.,*

2021, vol. 42, pp. 2018–2024.
https://doi.org/10.1016/j.matpr.2020.12.253

9. Zhang, X., Xiao, B., and Ma, Z., A transient thermal model for friction stir weld. Part I: the model, *Metall. Mater. Trans. A,* 2011, vol. 42, no. 10, pp. 3218–3228.
https://doi.org/10.1007/s11661-011-0729-5
10. Nunes, A., Heat input and temperature distribution in friction stir welding, *Month,* 1998, pp. 163–172. Tang, W., Guo, X., McClure, J.C., Murr, L.E., and Nunes, A.C., Heat input and temperature distribution in friction stir welding, *J. Mater. Process. Manuf. Sci.,* 1998, vol. 7, no. 2, pp. 163–172.
11. Song, M. and Kovacevic, R., Heat transfer modelling for both workpiece and tool in the friction stir welding process: a coupled model, *Proc. Inst. Mech. Eng., Part B,* 2004, vol. 218, no. 1, pp. 17–33.
https://doi.org/10.1243/095440504772830174
12. Song, M. and Kovacevic, R., Thermal modeling of friction stir welding in a moving coordinate system and its validation, *Int. J. Mach. Tools Manuf.,* 2003, vol. 43, no. 6, pp. 605–615.
https://doi.org/10.1016/S0890-6955(03)00022-1
13. Nandan, R., Roy, G., and Debroy, T., Numerical simulation of three-dimensional heat transfer and plastic flow during friction stir welding, *Metall. Mater. Trans. A,* 2006, vol. 37, no. 4, pp. 1247–1259.
https://doi.org/10.1007/s11661-006-1076-9
14. Su, P., Gerlich, A., North, T., and Bendzsak, G., Energy utilization and generation during friction stir spot welding, *Sci. Technol. Weld. Joining,* 2006, vol. 11, no. 2, pp. 163–169.
https://doi.org/10.1179/174329306X84373
15. Mishra, S. and DebRoy, T., A heat-transfer and fluid-flow-based model to obtain a specific weld geometry using various combinations of welding variables, *J. Appl. Phys.,* 2005, vol. 98, no. 4, p. 044902.
https://doi.org/10.1063/1.2001153
16. Serier, M., Alazzawi, S., Chikh, A., Berrahou, M., Ahmad, T., Shihab, S.K., and Siddiquee, A.N., Parametric studies of friction stir welding with tool using a vibrating shoulder, *Mater. Today: Proc.,* 2022, vol. 62, pp. 70–76.
https://doi.org/10.1016/j.matpr.2022.02.136
17. Al-Sabur, R., Tensile strength prediction of aluminium alloys welded by FSW using response surface methodology—Comparative review, *Mater. Today: Proc.,* 2021, vol. 45, pp. 4504–4510.
https://doi.org/10.1016/j.matpr.2020.12.1001
18. Verduzco Juárez, J., Dominguez Almaraz, G., García Hernández, R., and Villalón López, J., Effect of modified pin profile and process parameters on the friction stir welding of aluminum alloy 6061-T6, *Adv. Mater. Sci. Eng.,* 2016, vol. 2016, p. 4567940.
https://doi.org/10.1155/2016/4567940
19. Hamilton, C., Dymek, S., and Sommers, A., A thermal model of friction stir welding in aluminum alloys, *Int. J. Mach. Tools Manuf.,* 2008, vol. 48, no. 10, pp. 1120–1130.
https://doi.org/10.1016/j.ijmachtools.2008.02.001
20. Louvet, F. and Delplanque, L., *Design of Experiments: The French Touch,* Orléans: Experimentique, 2005.
21. Goupy, J., *Pratiquer les plans d'expériences,* Dunod, 2005.